Journal of Power Sources 239 (2013) 584–595

Contents lists available at SciVerse ScienceDirect

Journal of Power Sources

journal homepage: www.elsevier.com/locate/jpowsour

Model-based behaviour of a high temperature electrolyser system operated at various loads

Floriane Petipas [a,b,*], Annabelle Brisse [a], Chakib Bouallou [b]

[a] European Institute For Energy Research (EIFER), Emmy-Noether-Strasse 11, 76131 Karlsruhe, Germany
[b] MINES ParisTech, Centre for Energy efficiency of Systems (CES), 60 Boulevard Saint Michel, 75006 Paris, France

HIGHLIGHTS

- Dynamic model of an SOEC system operated at different loads.
- Stable system efficiency of 91% vs. HHV considering no external heat source.
- System power 80% dedicated to electrolysis and 15% dedicated to electrical heating.
- System power load ranged from 60% to 100%.
- Necessity of complementary control strategies to enlarge the load range.

ARTICLE INFO

Article history:
Received 18 October 2012
Received in revised form
1 March 2013
Accepted 6 March 2013
Available online 19 March 2013

Keywords:
High temperature electrolysis
Dynamic model
System integration
Variable operation
Hydrogen production

ABSTRACT

The objective of this study is to describe the steady-state behaviour of a Solid Oxide Electrolysis Cell (SOEC) system operated at different power loads without an external heat source and producing compressed hydrogen (3 MPa). A zero-dimensional model is proposed to describe the system, which is composed of an SOEC unit and a Balance of Plant. Results found that the system efficiency equals 91% vs. HHV and is slightly impacted by the operating load. However, due to the SOEC sensitivity to thermal gradients, the SOEC unit has to be operated close to the thermoneutral mode, which restricts the SOEC system power load to the range 60–100%. Control strategies, such as additional heating and independently operated SOEC units, should be employed below 60% load to enable the electrolyser operation across a wider load range.

1. Introduction

1.1. Need for interconnected energy networks

In 2010, the fossil fuels consumption accounted for 82% of the world energy consumption, shared between oil (34%), coal (26%) and gas (22%), whilst the contribution of renewables was 13%, dominated by biomass [1]. Many issues related to the fossil fuel based economy, such as global warming, air pollution, fuel reserves depletion or countries energetic dependence, motivate an evolution of the current energy system through the gradual replacement of fossil fuels by renewables, such as biomass, wind and solar.

In the European Union (EU), the 20–20–20 targets aim to achieve a 20% share of renewables in the energy mix as well as a 20% reduction of CO_2 emissions and a 20% increase in energy efficiency by 2020 with respect to the 1990 levels. Following these targets, the renewables installed capacity has increased from 22.7% (130 GW) in 2000 to 31.3% (280 GW) in 2011, which was driven by the exponential deployment of wind turbines (2.2–10.5%) and photovoltaic panels (0.0–5.1%) [2].

However, the introduction of large amounts of intermittent electricity into the current electrical grid creates grid instability issues that need to be solved through the development of a smart grid management based on interconnected energy networks. While storing large amounts of electrical energy is a challenge, storing large amounts of gas is not an issue since the gas storage capacity is generally considered as infinite. Therefore, the Power-to-Gas concept proposes to interconnect the electricity and gas networks in order to store excess electrical energy as gas [3]. Moreover, the interconnection with a heat network could maximise the processes

* Corresponding author. European Institute For Energy Research (EIFER), Emmy-Noether-Strasse 11, 76131 Karlsruhe, Germany. Tel.: +49 721 6105 1716; fax: +49 721 6105 1332.
E-mail addresses: petipas@eifer.org (F. Petipas), brisse@eifer.org (A. Brisse), chakib.bouallou@mines-paristech.fr (C. Bouallou).

0378-7753/$ – see front matter © 2013 Elsevier B.V. All rights reserved.
http://dx.doi.org/10.1016/j.jpowsour.2013.03.027

Nomenclature

ASR_T	stack Area Specific Resistance at a given temperature ($\Omega\,cm^2$)
$c_{p_{gas}T}$	constant pressure molar heat capacity of a given gas at a given temperature ($J\,mol^{-1}\,K^{-1}$)
e_{cell}	single-repeated unit thickness (m)
$e_{endplate}$	endplate thickness (m)
$e_{insulation}$	insulation thickness (m)
E, E_N	cell voltage, cell Nernst voltage (V)
F	Faraday's constant (96,485 $C\,mol^{-1}$)
HHV	Higher Heating Value of hydrogen (286,000 $J\,mol^{-1}$)
j	cell current density ($A\,cm^{-2}$)
K_s	cell heat capacity ($J\,K^{-1}$)
ℓ_{cell}	cell length (m)
ℓ_{stack}	stack length including manifolds (m)
$\dot{n}$, $\dot{N}$	cell, total molar flow rate of produced hydrogen ($mol\,s^{-1}$)
$\dot{n}_{gas}$, $\dot{N}_{gas}$	cell, total molar flow rate of a given gas ($mol\,s^{-1}$)
N_{cell}	number of cells per unit
N_{cell_stack}	number of cells per stack
N_{stack}	number of stacks per unit
N_{stage}	number of compression stages
$p_{c,1}$, $p_{c,2}$	inlet, outlet pressure of a compression stage (MPa)
p_{gas_in}, p_{gas_out}, p_{gas}	cell inlet, outlet, average partial pressure of a given gas
p_{out}	hydrogen pressure at the outlet of the system (MPa)
$p_{p,1}$, $p_{p,2}$	inlet, outlet pressure of the pumped water (MPa)
P_{BoP_heater}, P_{BoP_pump}	BoP heater, BoP pump power (W)
P_{cell}	cell power (W)
$P_{compressor}$	compressor power (W)
P_{gas_in}, P_{gas_out}	cell inlet, outlet gases thermal power (W)
P_{unit_loss}	unit heat losses (W)
$P_{reaction}$	cell power required for the reaction (W)
$P_{th\_heating}$, $P_{th\_cooling}$	heating, cooling BoP thermal power (W)
R	ideal gas constant ($8.314\,J\,mol^{-1}\,K^{-1}$)
R_{air}	air ratio
S_{active}	cell active surface area (cm^2)
SC	steam conversion rate
S_{unit}	unit insulated surface (m^2)
t	time (s)
T	considered temperature (K)
T_{amb}	ambient temperature (K)
$T_{c,1}$, $T_{c,2}$	inlet, outlet temperature of a compression stage (K)
$T_{filtration}$	hydrogen filtration temperature (K)
T_{in}, T_{out}, T_{cell}	cell inlet, outlet, average temperature (K)
$T_{p,1}$, $T_{p,2}$	inlet, outlet temperature of the pumped water (K)
T_{source}	water temperature at the inlet of the system (K)
V_{unit_th}	theoretical volume of the unit (m^3)
Z_{stage}	average hydrogen compression factor for a given stage

Greek letters

ΔH_{vap}	water enthalpy of vaporisation (40,668 $J\,mol^{-1}$)
ΔP_{cold_gases}, ΔP_{hot_gases}	cold, hot streams required thermal power (W)
ΔP_{gas}	required thermal power of a given gas (W)
ΔP_{vap}	phase transition required thermal power (W)
$\Delta_r G_T^0$	standard Gibbs free energy change of reaction at a given temperature ($J\,mol^{-1}$)
$\Delta_r H_T$	enthalpy change of reaction at a given temperature ($J\,mol^{-1}$)
δT	temperature difference in the pinch analysis (K)
ΔT	temperature gradient across the cell (K)
ΔT_{cell}	cell temperature variation between two iterations (K)
ε	coefficient used in the ASR equation ($\Omega\,cm^2$)
η_{BoP_heater}, η_{BoP_pump}	BoP heater, BoP pump efficiency
$\eta_{isentropic}$, $\eta_{mechanical}$	isentropic, mechanical efficiency of compression
η_{system}	SOEC system efficiency
κ_{stage}	hydrogen average heat capacity ratio for a given stage
λ_T	insulation thermal conductivity at a given temperature ($W\,m^{-1}\,K^{-1}$)

Indices

H_2, N_2, O_2	hydrogen, nitrogen, oxygen
$H_2O_{(l)}$, $H_2O_{(g)}$, H_2O	liquid water, steam, water

efficiency, which is developed in combined heat and power (CHP) plants and micro-CHP systems. Fig. 1 shows a possible 100% renewables based energy system, where the electricity, natural gas and heat networks are smartly interconnected in order to reach the highest efficiency.

1.2. Electrolysis

Independently from the hydrogen final use, the production of hydrogen from renewable electrical energy is performed within an electrolyser which should be flexible, efficient and affordable for electrolysis to become a cost-effective solution. The electrolysis reaction can be conducted below 373 K with liquid water using an Alkaline ELectrolyser (AEL) or a Proton Exchange Membrane ELectrolyser (PEMEL), or above 773 K with steam using a High Temperature ELectrolyser (HTEL, based on Solid Oxide Electrolysis Cells, SOECs).

Electrolysis is an endothermic reaction, thus both electrical and thermal energy must be provided. At the thermoneutral voltage (1.481 V at 298 K and 1.286 V at 1073 K), the electrolyser material Joule heating balances the reaction thermal energy needs. The cell electrical efficiency, which is the hydrogen Higher Heating Value (HHV) divided by the enthalpy change of reaction, equals 100% vs. HHV at 298 K and 115% vs. HHV at 1073 K. Cell efficiency values above 100% vs. HHV are obtained because of the definition of the HHV. Indeed, the HHV corresponds to the heat which can be recovered from the hydrogen combustion including the latent heat of condensation of water, without taking into account the temperature of the gases. Hence, when the temperature of the electrolyser is higher than 298 K, the reaction efficiency is greater than 100% vs. HHV.

Above the thermoneutral voltage (exothermic mode), the electrolyser material Joule heating is greater than the reaction thermal energy needs, hence the dissipation of excess heat causes a cell electrical efficiency decrease. Low temperature electrolysers are usually operated largely above the thermoneutral voltage (1.7–2.0 V), whereas SOECs operate usually much closer to the thermoneutral voltage, in the range 1.1–1.5 V, which leads to much higher cell electrical efficiencies, hence rendering HTEL a very promising technology.

Several studies are focusing on high temperature electrolysis coupled with renewable energy sources for the production of carbon-free hydrogen [4–7]. However, the behaviour of SOEC systems under various power loads and without an external heat source has not been reported yet. The present study addresses this issue through the use of an SOEC system model.

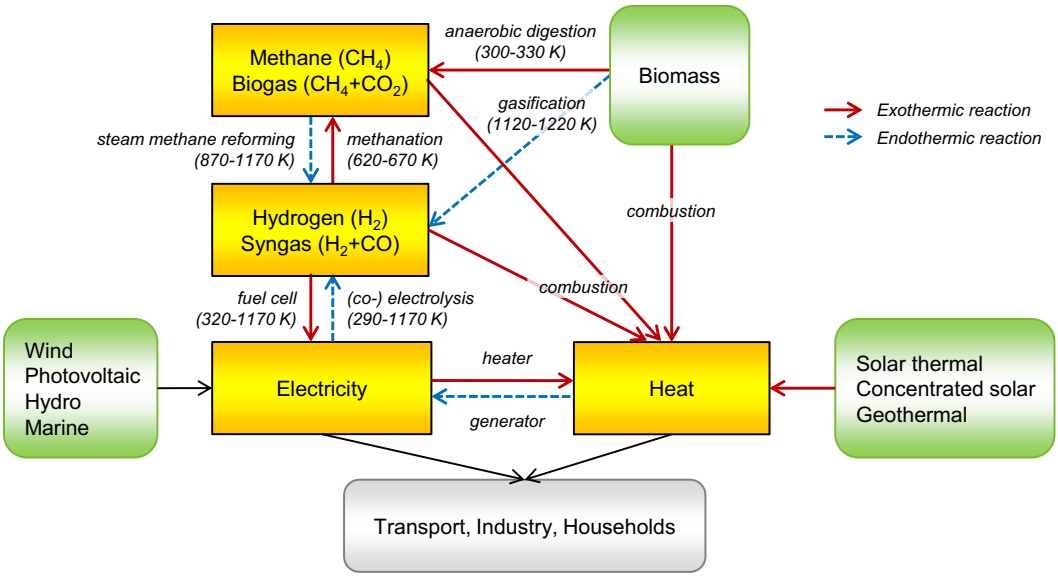

Fig. 1. 100% renewables based energy system based on interconnections between energy networks.

2. Model

At the cell and stack level, most models found in the literature were one-dimensional models [8–11], describing the parameters evolution along the cell. For the calculation, the cell length was divided into small sections in which the cell voltage, gas flow rates and temperatures were calculated with an iterative method. In the operating range considered for practical operation, the calculated current density, voltage and temperature were quasi-linear along the cell [8,10] in spite of complex one-dimensional calculation. In the present work aiming to describe a system, a zero-dimensional model is therefore considered to be accurate enough.

Moreover, due to the lack of experimental data, white-box models (based on physical equations) were usually proposed in the literature. Overvoltages were then described in detail, based on the Butler–Volmer equation for the calculation of activation overvoltages, the Ohm's law for the calculation of the ohmic losses, and the Fick's law for the calculation of the concentration overvoltages. On the contrary, when experimental data were available, grey-box models (based on both physical equations and experimental data) could be proposed, which was the case of O'Brien et al. [11] and Fu et al. [12] who both used expressions of the Area Specific Resistance (ASR) as a function of the temperature, derived from experimental data.

In the present work, a zero-dimensional grey-box model developed in Simulink® is proposed. For the purposes of this study, only results obtained in steady state are displayed.

The model is composed of two coupled submodels describing the electrolyser module and the Balance of Plant (BoP), respectively. Fig. 2 shows a schematic representation of the modelled configuration. In order to compare the calculated system efficiency with typical low temperature electrolysis processes operating under pressure, no external heat source is provided and the produced hydrogen is compressed from the atmospheric pressure to 3 MPa. Due to the high operating temperature, steam has to be provided to the electrolyser module. The corresponding heat requirements are covered in the BoP by an efficient recovery of the outlet gases heat and of the compression heat, as well as by electrical heating. Model input parameters and operating conditions implemented in this work are displayed in Table 1.

2.1. Electrolysis cell submodel

2.1.1. Electrolyser module

The definition of the SOEC system hierarchy is very important for a clear understanding of the terms used in this work. In particular, SOE cells are assembled to form SOEC stacks, which are connected to form an insulated SOEC unit. Although only one unit is used in this work, several units could be used and form one SOEC module. Finally, the Balance of Plant module is integrated and the combination of the SOEC module and the BoP module is called the SOEC system.

The electrolyser module is composed of one unit of 10,000 cells (N_{cell}) operating at the atmospheric pressure and at the average temperature (T_{cell}) of $T_{in} \pm \Delta T/2$, corresponding in this work to 1073 ± 50 K. The Solid Oxide Electrolysis Cells are assumed to have an active surface area (S_{active}) of 100 cm^2.

Fig. 3 shows the scale-up of the cell to the unit. An insulation wall (thickness $e_{insulation}$) is implemented around the SOEC unit to limit heat losses. The required insulation surface (S_{unit}) is minimised through a quasi-cubic unit design, calculated as follows. The cell is assumed to be a 0.152 m (ℓ_{cell}) side square, as given for a cell of 100 cm^2 active surface area in [13]. Around the cells, a space of 0.02 m is additionally considered for manifolds, therefore a 0.192 m (ℓ_{stack}) side square is considered. Each single-repeated unit has a thickness of e_{cell} (0.003 m), and spaces of $e_{endplate}$ (0.05 m) at the bottom and at the top of the stacks are additionally considered for endplates and manifolds. For the distribution of the cells among stacks, the unit is first considered as one stack of N_{cell} cells, corresponding to the volume (V_{unit_th}) given in Eq. (1). Since stacks should not be piled up to enable access at the top and at the bottom for electrical and gas connections as well as for maintenance, cells are distributed among adjacent stacks, hence the unit edge equals the volume cube root. Since a perfectly cubic configuration is usually not feasible, the number of stacks per unit (N_{stack}) is calculated by rounding the volume cube root, as in Eq. (2), and the number of cells per stack (N_{cell_stack}) is calculated as in Eq. (3). Because a fixed number of cells per stack is considered, the total number of cells per unit (N_{cell}) has to be adjusted, see Eq. (4). Finally, the quasi-cubic unit external surface (S_{unit}) is given in Eq. (5). In this work, the unit is composed of 25 adjacent stacks of 400 cells each, corresponding to a

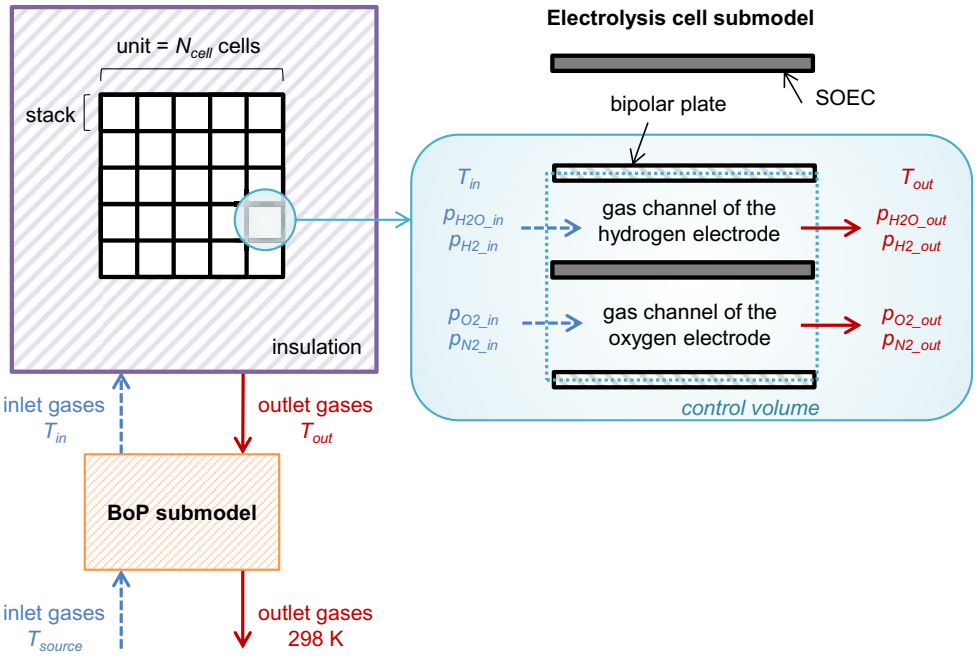

Fig. 2. Schematic representation of the modelled configuration.

unit volume of $96 \times 96 \times 130\ cm^3$ and a thermally insulated surface (S_{unit}) of 6.84 m^2.

$$V_{unit\_th} = (\ell_{stack})^2 \cdot \left(N_{cell} \cdot e_{cell} + 2 \cdot e_{endplate}\right) \quad (1)$$

$$N_{stack} = \text{round}\left(\frac{\sqrt[3]{V_{unit\_th}}}{\ell_{stack}}\right)^2 \quad (2)$$

$$N_{cell\_stack} = \text{round}\left(\frac{N_{cell}}{N_{stack}}\right) \quad (3)$$

$$N_{cell} = N_{cell\_stack} \cdot N_{stack} \quad (4)$$

$$S_{unit} = 4 \cdot \sqrt{N_{stack}} \cdot \ell_{stack} \cdot \left(N_{cell\_stack} \cdot e_{cell} + 2 \cdot e_{endplate}\right) + 2 \cdot N_{stack} \cdot (\ell_{stack})^2 \quad (5)$$

The thermal insulation is made of the microporous high temperature insulation material Microtherm 240 kg m^{-3} (Microtek International Ltd.), whose thermal conductivity (λ) is temperature dependent, as expressed for a given temperature T in Eq. (6), which is a polynomial fit of data collected between 273 K and 1273 K in [14]. Heat convection at the insulation surface is assumed to be negligible, which implies that the internal surface temperature equals the average cell temperature (T_{cell}) and the external surface temperature equals the ambient temperature (T_{amb}). The temperature evolution within the insulation is assumed to be linear, hence the thermal conductivity (λ) is calculated using the average insulation temperature.

$$\lambda_T = 2.09 \cdot 10^{-2} - 4.07 \cdot 10^{-6} \cdot T + 1.30 \cdot 10^{-8} \cdot T^2 \quad (6)$$

2.1.2. Heat capacity

The specific heat capacity of a stack is usually 400–500 J kg^{-1} K^{-1} [8,14,15]. Since the heat capacity is calculated from the solid parts volume, the stack heat capacity is highly dependent on the design, in particular on the gas channels design in bipolar plates. The considered value for the cell heat capacity (K_s) is 96.86 J K^{-1}, as given in [15] for a single-repeated unit whose dimensions were similar to those considered in this work.

Table 1
Model input parameters and operating conditions implemented in this work.

ASR	0.5 Ω cm^2 at 1073 K
e_{cell}	0.003 m
$e_{endplate}$	0.05 m
$e_{insulation}$	0.3 m
K_s	96.86 J K^{-1}
ℓ_{stack}	0.192 m
N_{cell}	10,000
N_{stage}	2
$p_{c,1}$	0.1/0.55 MPa
$p_{c,2}$	0.55/3 MPa
$p_{H_2O\_in}$	100%
$p_{H_2\_in}$	0%
$p_{N_2\_in}$	0%
$p_{O_2\_in}$	100%
p_{out}	3 MPa
$p_{p,1} - p_{p,2}$	0.01 MPa
R_{air}	0
S_{active}	100 cm^2
SC	75%
T_{amb}	288 K
$T_{c,1}$	298 K
$T_{filtration}$	298 K
T_{in}	1073 K
$T_{p,1}$	288 K
$T_{p,2}$	298 K
T_{source}	288 K
Z_{stage}	1.0015/1.0081
Greek letters	
δT	40 K
ΔT	100 K
κ_{stage}	1.4010/1.4012
η_{BoP_heater}	95%
η_{BoP_pump}	75%
$\eta_{isentropic}$	75%
$\eta_{mechanical}$	90%

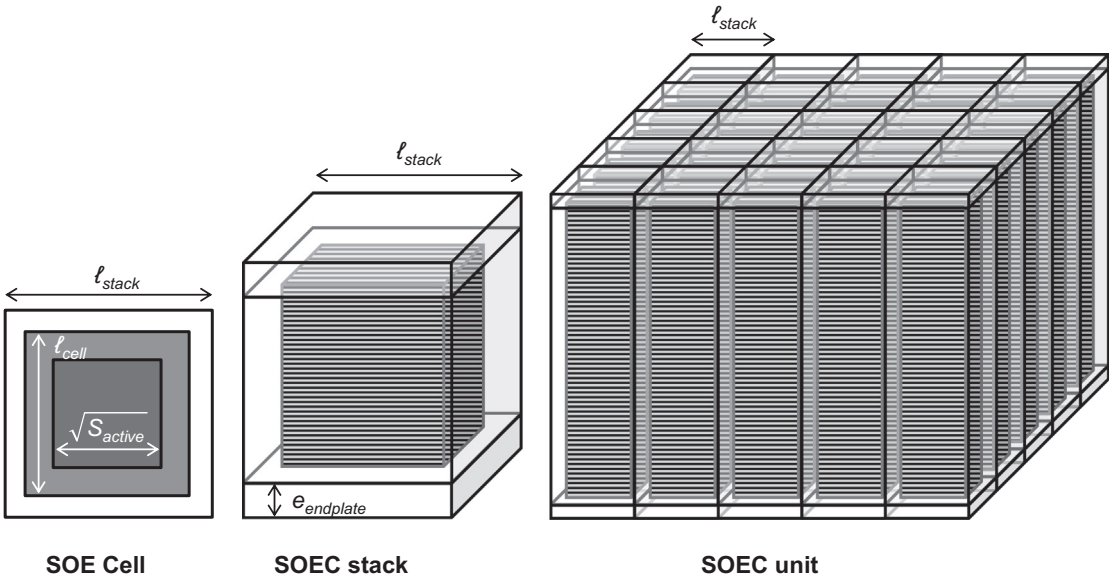

Fig. 3. Scale-up of the cell to the unit.

2.1.3. Gas composition

Each cell is fed with gases preheated to 1073 K (T_{in}). Due to the presence of nickel in the hydrogen electrode, a reducing atmosphere has to be maintained. As hydrogen is constantly being produced during the electrolyser operation, a 100% steam inlet gas can be assumed not to degrade the electrode. When the electrolyser is stopped, hydrogen should be however introduced at the hydrogen electrode before standby or shut-down. The inlet steam and hydrogen partial pressures are noted $p_{H_2O\_in}$ and $p_{H_2\_in}$. They equal, respectively, 100% and 0% in this work.

The steam conversion rate (*SC*) represents the ratio of steam which is split into hydrogen and oxygen. To avoid energy waste associated to preheated steam flowing through the cell without reacting, the conversion rate should be as high as possible. However, above 90%, localised steam starvation occurs due to the large presence of produced hydrogen at the hydrogen electrode, which should be avoided [16]. Conversion rate values used in reported modelling works are usually in the range 75–80% [7,8,18]. A conversion rate of 75% is assumed to be an acceptable compromise and is integrated in the model. As the quantity of reacted steam is proportional to the current, a constant conversion rate implies that any variation in the current input will induce a proportional variation in the inlet steam flow rate.

At the oxygen electrode, air sweep could be considered using the air ratio (R_{air}), defined as the ratio between the oxygen inlet flow rate contained in the air sweep, to the oxygen production rate, as defined in [19]. In this work, no air sweep is used in order to increase the system efficiency [12,16] and the air-sweep feed is closed to allow the produced oxygen to flow out at the outlet. The presence of pure hydrogen and pure oxygen is assumed to cause no safety issue in the system.

2.1.4. Operating temperature range

The inlet temperature is assumed to be constant at T_{in} (1073 K), whilst the outlet temperature (T_{out}) depends on the operating mode (endothermic, thermoneutral or exothermic).

Because the probability of cell failure increases significantly for thermal gradients above 10 K cm^{-1} [20], the maximum tolerable temperature gradient across the cell (ΔT) is set to be ±100 K, which corresponds to an outlet temperature of 1073 ± 100 K. As the cell temperature is assumed to equal the average of the inlet and the outlet temperatures, the cell should be operated in the range of 1073 ± 50 K to prevent from mechanical failures. Due to this large temperature range, the temperature dependence of several parameters is taken into account with feedback loops in order to increase the results accuracy, as detailed hereafter.

2.1.5. Area specific resistance

The Area Specific Resistance (*ASR*) is a key parameter in the electrolyser performance since it represents the irreversible losses. The equation of Fu et al. [12] described the cell ASR temperature dependence around 1073 K, based on data measured on an SOEC for which the ASR was 0.25 Ω cm^2 at 1073 K. The ASR temperature dependence can be assumed to be similar for a stack and a cell, therefore an adapted version of the Fu et al. [12] equation, using the coefficient ε to shift the curve and meet the required stack ASR value at 1073 K, is implemented as given in Eq. (7). Since ASR values are higher for a stack than for a cell, a stack ASR value of 0.5 Ω cm^2 at 1073 K is used in the model, with ε corresponding to 0.25 Ω cm^2. This value is considered to be achievable in the short run, since the ASR measured on a 25-cell stack was already around 0.8 Ω cm^2 in 2010 [21].

$$ASR_T = \exp(4900/T - 5.95) + \varepsilon \tag{7}$$

2.1.6. Further temperature dependent parameters

Further temperature dependent parameters used in the model are the enthalpy change of reaction $\Delta_r H$, the standard Gibbs free energy change of reaction $\Delta_r G^0$ and the molar heat capacity c_p of the gases, whose temperature dependence is given in Eqs. (8)–(14), fitted from data collected in [22]. Eqs. (8), (9) and (11) apply above 373 K, whereas Eq. (10) applies below 373 K.

$$\Delta_r H_T = 238,200 + 13.12 \cdot T - 3.55 \cdot 10^{-3} \cdot T^2 \tag{8}$$

$$\Delta_r G_T^0 = 244,800 - 49.18 \cdot T - 2.72 \cdot 10^{-3} \cdot T^2 \tag{9}$$

$$c_{p_{H_2O_{(l)}T}} = 92.67 - 1.11 \cdot 10^{-1} \cdot T + 1.78 \cdot 10^{-4} \cdot T^2 \tag{10}$$

$$c_{p_{H_2O_{(g)}T}} = 113.2 - 5.18\cdot10^{-1}\cdot T + 1.32\cdot10^{-3}\cdot T^2 - 1.63\cdot10^{-6}\cdot T^3 + 9.86\cdot10^{-10}\cdot T^4 - 2.36\cdot10^{-13}\cdot T^5 \quad (11)$$

$$c_{p_{H_2T}} = 22.00 + 5.19\cdot10^{-2}\cdot T - 1.44\cdot10^{-4}\cdot T^2 + 1.93\cdot10^{-7}\cdot T^3 - 1.22\cdot10^{-10}\cdot T^4 + 3.02\cdot10^{-14}\cdot T^5 \quad (12)$$

$$c_{p_{O_2T}} = 30.11 - 1.47\cdot10^{-2}\cdot T + 5.54\cdot10^{-5}\cdot T^2 - 5.18\cdot10^{-8}\cdot T^3 + 1.59\cdot10^{-11}\cdot T^4 \quad (13)$$

$$c_{p_{N_2T}} = 30.64 - 1.06\cdot10^{-2}\cdot T + 2.16\cdot10^{-5}\cdot T^2 - 8.91\cdot10^{-9}\cdot T^3 \quad (14)$$

2.1.7. Assumptions

Average cell values, calculated as the mean of inlet and outlet values as expressed in Eqs. (15) and (16) for the temperature and the partial pressures, are assumed to be representative of the cell.

$$T_{cell} = (T_{in} + T_{out})/2 \quad (15)$$

$$p_{gas} = \left(p_{gas\_in} + p_{gas\_out}\right)/2 \quad (16)$$

Moreover, the following assumptions are made in the electrolysis cell submodel:

- Initial condition: no reaction (outlet values equal inlet values).
- Pressure drop neglected.
- Electrochemistry and mass transfer dynamics neglected.
- Solid temperature equals gas temperature.
- Average cell values representative of the entire unit.

2.1.8. Mass and energy balances

The electrolysis cell submodel combines mass and energy balances calculated iteratively with two feedback loops, as shown in the flowchart of Fig. 4, where the principal loop is iterated until ΔT_{cell} converges, and the secondary loop is iterated five times to ensure convergence. Typical flowchart symbols are used, in particular parallelograms for inputs/outputs, rectangles for generic processing steps, diamonds for conditionals and circles for ending the simulation of time "t".

The Nernst voltage (E_N or Open Circuit Voltage, OCV), the cell current density (j) and the cell voltage (E) are first calculated in the middle of the cell using Eqs. (17)–(19). These calculations are based on the cell power (P_{cell}) which is the unit power divided by the number of cells per unit. The Area Specific Resistance (ASR) and the standard Gibbs free energy change of reaction ($\Delta_r G^0$) are calculated at the cell temperature (T_{cell}) as defined in Eqs. (7) and (9). The partial pressures of the gases (p_{H_2}, p_{O_2} and p_{H_2O}) are calculated iteratively in the middle of the cell. Since average cell values are assumed to be representative of the entire cell and since initial conditions correspond to the inlet values, a few iterations are required for the calculation to converge.

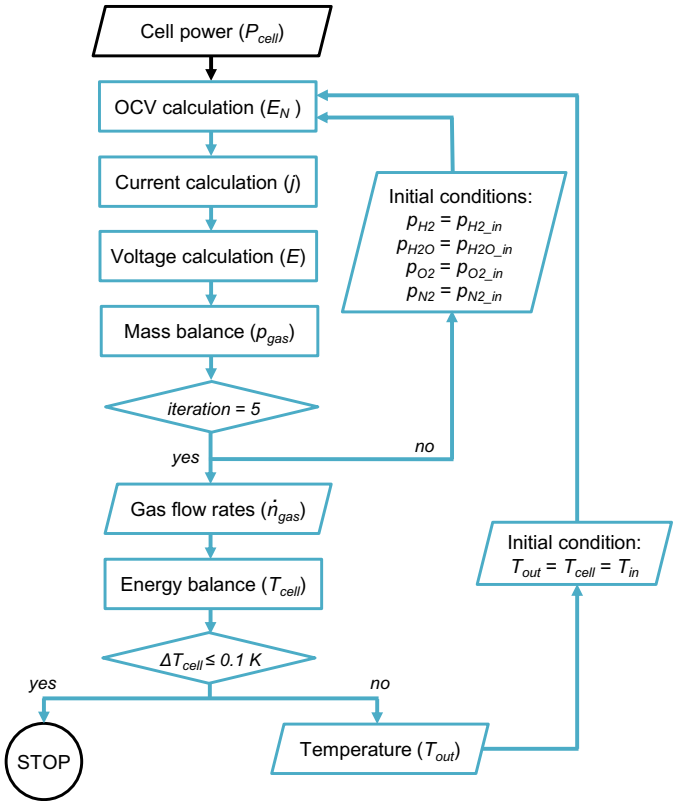

Fig. 4. Flowchart of the electrolysis cell submodel, whose outputs are the gas flow rates and the outlet temperature.

$$E_N = \frac{\Delta_r G^0_{T_{cell}}}{2\cdot F} + \frac{R\cdot T_{cell}}{2\cdot F}\cdot\ln\left(\frac{p_{H_2}\cdot\sqrt{p_{O_2}}}{p_{H_2O}}\right) \quad (17)$$

$$j = \frac{E_N}{2\cdot ASR_{T_{cell}}} + \sqrt{\frac{P_{cell}}{S_{active}\cdot ASR_{T_{cell}}} + \left(\frac{E_N}{2\cdot ASR_{T_{cell}}}\right)^2} \quad (18)$$

$$E = E_N + j\cdot ASR_{T_{cell}} \quad (19)$$

The mass balance is based on the Faraday's law of electrolysis, which enables to calculate the molar flow rate of produced hydrogen or reacted steam ($\dot{n}$), as detailed in Eq. (20). Inlet and outlet gas molar flow rates are calculated in Eqs. (21)–(28) using the steam conversion rate (SC) and the air ratio (R_{air}).

$$\dot{n} = \frac{j\cdot S_{active}}{2\cdot F} \quad (20)$$

$$\dot{n}_{H_2O_{in}} = \frac{\dot{n}}{SC} \quad (21)$$

$$\dot{n}_{H_2O_{out}} = \dot{n}_{H_2O_{in}} - \dot{n} \quad (22)$$

$$\dot{n}_{H_{2_{in}}} = \dot{n}_{H_2O_{in}}\cdot\frac{p_{H_2\_in}}{p_{H_2O\_in}} \quad (23)$$

$$\dot{n}_{H_{2_{out}}} = \dot{n}_{H_{2_{in}}} - \dot{n} \quad (24)$$

$$\dot{n}_{O_{2_{in}}} = 0.5 \cdot \dot{n} \cdot R_{air} \quad (25)$$

$$\dot{n}_{O_{2_{out}}} = \dot{n}_{O_{2_{in}}} + 0.5 \cdot \dot{n} \quad (26)$$

$$\dot{n}_{N_{2_{in}}} = \dot{n}_{O_{2_{in}}} \cdot \frac{p_{N_2\_in}}{p_{O_2\_in}} \quad (27)$$

$$\dot{n}_{N_{2_{out}}} = \dot{n}_{N_{2_{in}}} \quad (28)$$

The cell temperature is calculated by performing an energy balance between the inlet and the outlet of the cell, as shown in Eq. (29). The thermal power stored in the cell corresponds to the thermal variation (dT_{cell}/dt) multiplied by the heat capacity (K_s). This thermal power is calculated using the cell power (P_{cell}), the power absorbed by the reaction ($P_{reaction}$), the inlet and outlet gases thermal powers (P_{gas_in} and P_{gas_out}), as well as the unit heat losses (P_{unit_loss}) divided by the number of cells per unit (N_{cell}).

$$K_s \frac{dT_{cell}}{dt} = P_{cell} + P_{reaction} + P_{gas\_in} + P_{gas\_out} + \frac{P_{unit\_loss}}{N_{cell}} \quad (29)$$

As detailed in Eq. (30), the power required for the reaction equals the produced hydrogen flow rate multiplied by the enthalpy change of reaction ($\Delta_r H$), which is calculated at the cell temperature (T_{cell}) from Eq. (8). The inlet and outlet gases thermal powers are calculated as shown in Eqs. (31) and (32), based on the gas heat capacities calculated at T_{in} and T_{out}, respectively, as given in Eqs. (11)–(14). The unit heat losses are calculated using the insulation thermal conductivity (λ), calculated in the middle of the insulation from Eq. (6), as well as the insulation thickness ($e_{insulation}$), the insulated surface (S_{unit}) and the temperature difference between the cell (T_{cell}) and the insulation external surface (T_{amb}) as given in Eq. (33).

$$P_{reaction} = -\dot{n} \cdot \Delta_r H_{T_{cell}} \quad (30)$$

$$P_{gas\_in} = (T_{in} - T_{cell}) \cdot \sum_{inlet\_gas} \left[c_{p_{inlet\_gas} T_{in}} \cdot \dot{n}_{inlet\_gas} \right] \quad (31)$$

$$P_{gas\_out} = -(T_{out} - T_{cell}) \cdot \sum_{outlet\_gas} \left[c_{p_{outlet\_gas} T_{out}} \cdot \dot{n}_{outlet\_gas} \right] \quad (32)$$

$$P_{unit\_loss} = -\frac{\lambda_{(T_{cell}+T_{amb})/2}}{e_{insulation}} \cdot S_{unit} \cdot (T_{cell} - T_{amb}) \quad (33)$$

2.2. Balance of Plant (BoP) submodel

BoP components can be divided into two categories: the mechanical BoP, comprising mechanical components such as pumps, and the electrical BoP, comprising electrical components such as rectifiers for the conversion of AC to DC. This study focuses exclusively on the mechanical BoP. Hence, the nomination BoP is assumed to correspond to the mechanical BoP.

The BoP submodel consists of a compression calculation and a pinch analysis, as detailed in the flowchart of Fig. 5 and as explained below.

2.2.1. BoP definition

The BoP encompasses the entire infrastructure that is required around the electrolyser to deliver steam preheated to T_{in} (1073 K) at the electrolyser module inlet, as well as pure hydrogen at the pressure p_{out} (3 MPa) and oxygen (mixed with nitrogen if air sweep is provided), both at 298 K, at the electrolyser system outlet. The

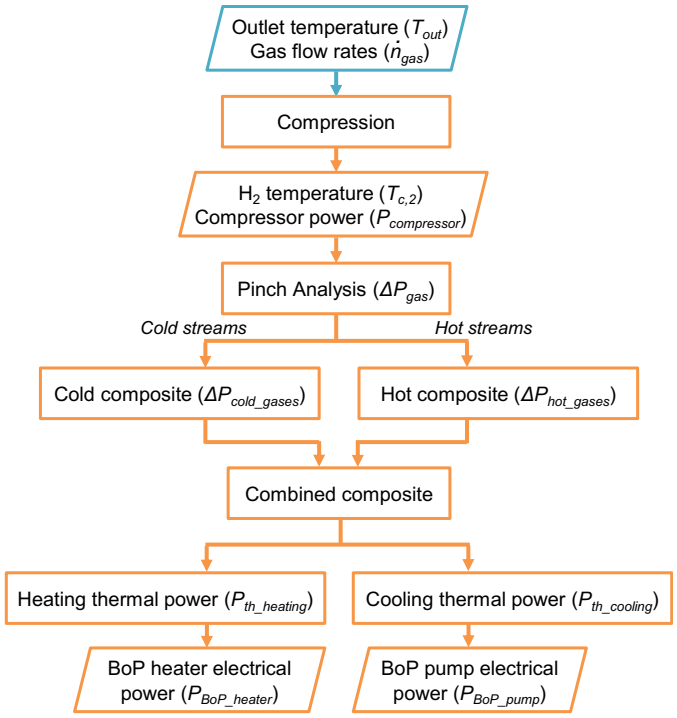

Fig. 5. Flowchart of the Balance of Plant submodel, whose outputs are the compressor, heater and pump powers.

BoP design aims to maximise the system efficiency. Total gas flow rates ($\dot{N}_{gas}$) are considered in the BoP and correspond to the cell flow rates calculated in the electrolysis cell submodel ($\dot{n}_{gas}$) multiplied by the number of cells per unit (N_{cell}), since the module is composed of only one unit in this work, as expressed in Eq. (34).

$$\dot{N}_{gas} = N_{cell} \cdot \dot{n}_{gas} \quad (34)$$

The model takes into account the temperature T_{source} (288 K) of the gases at the inlet of the system. Indeed, the gases could be preheated by an external heat source before entering the BoP in further works. Additionally, part of the power required to preheat the inlet gases from T_{source} to T_{in} is provided by recovering heat from the outlet gases, which are cooled down to 298 K.

2.2.2. Hydrogen compression

The compression can be performed either with a traditional compressor, which provides an isentropic compression, or with an ionic compressor [23], which enables an almost isothermal and thus more efficient compression. A traditional compressor, featuring an isentropic efficiency of 75% and a mechanical efficiency of 90%, is employed in the model. Heat dissipated through the hydrogen compression stage is however recovered to heat up the inlet gases.

Several compression stages, with intermediate gas cooling, are generally performed to approach an isothermal process. In this work, two compression stages (N_{stage}) are performed to achieve a compression from 0.1 MPa up to 3 MPa (p_{out}). Each stage increases the temperature from 298 K to $T_{c,2}$ (547 K), which is calculated from Eq. (35), where $T_{c,1}$ and $p_{c,1}$ are the hydrogen temperature and pressure before each compression stage, $p_{c,2}$ is the hydrogen pressure after each compression stage, $\eta_{isentropic}$ is the isentropic efficiency (75%) and κ_{stage} is the heat capacity ratio of hydrogen at the stage-average compression temperature. The power required to perform the compression ($P_{compressor}$) is calculated from Eq. (36), where $\dot{N}$ is the total hydrogen molar flow rate, Z_{stage} is the

compression factor of hydrogen at the stage-average pressure and temperature and $\eta_{\text{mechanical}}$ is the mechanical efficiency of the compression (90%).

$$T_{c,2} = T_{c,1} \cdot \left(1 + \frac{\left(p_{c,2}/p_{c,1}\right)^{\left(\kappa_{\text{stage}}-1\right)/\kappa_{\text{stage}}} - 1}{\eta_{\text{isentropic}}}\right) \tag{35}$$

$$P_{\text{compressor}} = \dot{N} \cdot \left(T_{c,2} - T_{c,1}\right) \cdot \frac{R}{\eta_{\text{mechanical}}} \cdot \sum_{\text{stage}} Z_{\text{stage}} \cdot \frac{\kappa_{\text{stage}}}{\kappa_{\text{stage}} - 1} \tag{36}$$

2.2.3. Hydrogen filtration

Hydrogen is basically separated from steam through steam condensation below 373 K in flash separators [18]. However, the BoP can be further optimised through the use of high temperature hydrogen filtration. Hydrogen can be indeed separated from steam between 623 K and 773 K with a palladium-based membrane. Once the separation is completed, the high temperature steam can be directly recycled to the electrolyser inlet, whilst only the hydrogen requires cooling to 298 K. Palladium-based membranes are hence a very promising technology for high temperature hydrogen production processes [24]. However, as the technology is at the research stage, traditional steam condensation performed below 373 K ($T_{\text{filtration}}$) is employed in this study.

2.2.4. Pinch analysis

The BoP components are not modelled in detail in this work. The BoP consumption is assumed to correspond to the compressor consumption as well as to the heating and cooling electrical consumptions. The BoP heating and cooling consumptions are minimised through the implementation of a pinch analysis. A pinch analysis is a method calculating the thermodynamically feasible minimum energy consumption which can be achieved in an optimised heat recovery system. To obtain a compromise between the surface area of the heat exchangers (thus their size and economical cost) and the ideal minimum energy consumption, the minimum tolerable temperature difference (δT) between hot and cold streams has to be defined, usually between 10 K and 40 K [25]. Due to the high temperature of the electrolysis process, the value is set to 40 K in this study.

All process streams are identified to calculate the thermal requirements. In the model, cold streams are inlet water ($\dot{N}_{H_2O_{in}}$), hydrogen ($\dot{N}_{H_{2_{in}}}$), oxygen ($\dot{N}_{O_{2_{in}}}$) and nitrogen ($\dot{N}_{N_{2_{in}}}$) which are heated from T_{source} to T_{in}. However in this work, the only cold stream is water, which is heated from 288 K to 373 K and vaporised before being overheated to 1073 K. Hot streams comprise:

- Unreacted steam ($\dot{N}_{H_2O_{out}}$), cooled down from T_{out} to 373 K and condensed before being further cooled down to 298 K.
- Outlet hydrogen ($\dot{N}_{H_{2_{out}}}$), cooled down from T_{out} to 298 K.
- Compressed hydrogen ($N_{\text{stage}} \cdot \dot{N}$), cooled down from $T_{c,2}$ to 298 K.
- Outlet oxygen ($\dot{N}_{O_{2_{out}}}$), cooled down from T_{out} to 298 K.
- Outlet nitrogen ($\dot{N}_{N_{2_{out}}}$), cooled down from T_{out} to 298 K.

Note that the compressed hydrogen flow rate ($N_{\text{stage}} \cdot \dot{N}$) does not correspond to the outlet but to the produced hydrogen flow rate multiplied by the number of compression stages. Indeed, in case hydrogen was injected in the inlet steam flow, a part of the outlet hydrogen would be directly recycled without being compressed.

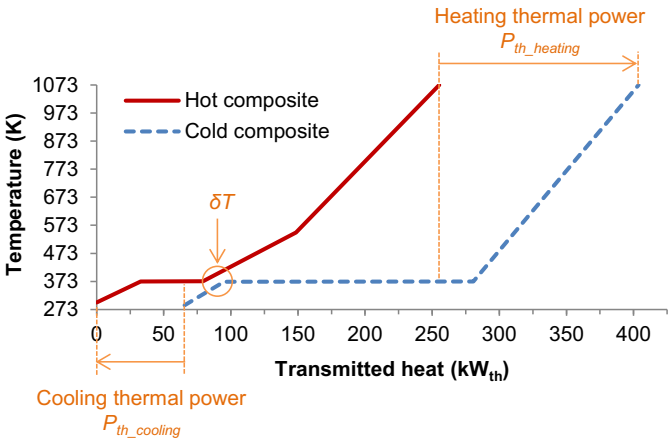

Fig. 6. Combined composite curve and optimised BoP requirements calculated at the thermoneutral power with the pinch analysis.

The required thermal power is calculated for each stream as expressed in Eq. (37), where $\dot{N}_{\text{gas}}$ is the gas molar flow rate, $c_{p_{\text{gas}}T}$ is the gas heat capacity as given in Eqs. (10)–(14), and dT is the temperature variation as indicated above.

$$\Delta P_{\text{gas}} = \dot{N}_{\text{gas}} \cdot \int c_{p_{\text{gas}}T} \cdot \mathrm{d}T \tag{37}$$

For water, the thermal power calculation is split into three steps, corresponding to the liquid phase, the phase transition and the gaseous phase. Eq. (37) is used for liquid water and for steam with the corresponding heat capacity values, whereas the water enthalpy of vaporisation (ΔH_{vap}) is used to calculate the phase transition thermal power, as in Eq. (38).

$$\Delta P_{\text{vap}} = \dot{N}_{H_2O} \cdot \Delta H_{\text{vap}} \tag{38}$$

These data define the cold composite curve and the hot composite curve, which are obtained by plotting the temperature against the calculated thermal power for cold streams and hot streams, respectively. The combined composite curve is composed of both composite curves separated by the minimum temperature difference (δT) on the temperature axis. The optimised utility requirements (heating power $P_{\text{th\_heating}}$ and cooling power $P_{\text{th\_cooling}}$) can be read on the thermal power axis and correspond to the areas where composite curves do not overlap. Fig. 6 shows the combined composite curve at the thermoneutral power

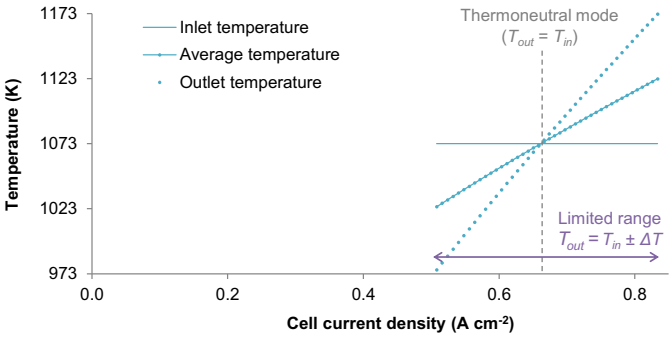

Fig. 7. Inlet, outlet and average temperatures as a function of the current density in steady state.

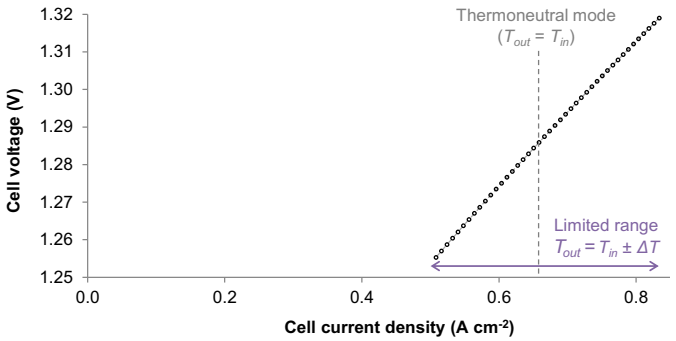

Fig. 8. Cell voltage as a function of the current density in steady state.

($T_{out} = T_{in}$): the inlet water (cold composite) is heated from T_{source} (288 K) to 373 K and is 85% vaporised by the heat recovery, before being further vaporised and overheated to T_{in} (1073 K) by an electrical heater ($P_{th\_heating} = 149\ kW_{th}$). Outlet gases (hot composite) are cooled down from T_{out} (1073 K) to 373 K and the steam is 30% condensed by the inlet gases. The outlet gases are further condensed and cooled down from 373 K to 298 K by pumped cooling water ($P_{th\_cooling} = 66\ kW_{th}$). The corresponding BoP thermal balance is expressed in Eq. (39), where ΔP_{cold_gases} and ΔP_{hot_gases} correspond to the calculated required thermal powers for cold and hot streams, respectively.

$$P_{th\_heating} + \Delta P_{hot\_gases} = P_{th\_cooling} + \Delta P_{cold\_gases} \quad (39)$$

2.2.5. BoP electrical consumption

The required heating power is provided by electrical heating, while the required cooling power is provided by pumped cooling water, whose temperature increases from 288 K ($T_{p,1}$) to 298 K ($T_{p,2}$) and whose pressure decreases by 0.01 MPa ($p_{p,1} - p_{p,2}$). The electrical powers P_{BoP_heater} and P_{BoP_pump} are calculated using Eqs. (40) and (41), where the electrical heater and the water pump have assumed efficiencies of 95% (η_{BoP_heater}) and 75% (η_{BoP_pump}), respectively.

$$P_{BoP\_heater} = \frac{P_{th\_heating}}{\eta_{BoP\_heater}} \quad (40)$$

$$P_{BoP\_pump} = \frac{p_{p,1} - p_{p,2}}{\eta_{BoP\_pump}} \cdot \frac{P_{th\_cooling}}{T_{p,2} \cdot c_{p_{H_2O_{(l)}T_{p,2}}} - T_{p,1} \cdot c_{p_{H_2O_{(l)}T_{p,1}}}} \quad (41)$$

In further developments of the presented model, detailed BoP designs could be implemented and already existing Heat Recovery Steam Generators (HRSG) should be considered [26]. Under intermittent operating conditions, the use of a Once Through Steam Generator (OTSG), a special type of HRSG without any boiler drum, may increase the process flexibility. This design allows quick variations in steam production rates, which is preferable under intermittent operation for the steam flow rate to follow the current variations.

2.3. System efficiency calculation

The total power of the SOEC system corresponds to the sum of the electrolyser module power and the BoP power. Since the model does not describe the electrical BoP, the power consumption of the power converter or electronic components is not taken into account. The system efficiency (η_{system}) is calculated by multiplying the hydrogen Higher Heating Value (HHV) by the total flow rate of produced hydrogen ($\dot{N}$), divided by the overall system power as detailed in Eq. (42).

$$\eta_{system} = \frac{\dot{N} \cdot HHV}{P_{cell} \cdot N_{cell} + P_{compressor} + P_{BoP\_heater} + P_{BoP\_pump}} \quad (42)$$

3. Results and discussion

The presented model was run at different system power loads in order to describe the system behaviour in steady state and to identify potential issues related to variable operation.

3.1. Electrolyser behaviour

At the electrolyser unit level, the cell power (P_{cell}) has a strong impact on the operating temperature. Fig. 7 displays the evolution of the outlet and average temperatures as a function of the applied current, whilst the cell inlet temperature is constant at 1073 K. As the outlet temperature needs to be in the range 1073 ± 100 K to avoid thermal stresses, the applicable current density ranges from 0.504 A cm^{-2} to 0.835 A cm^{-2}, which corresponds to cell voltages comprised between 1.255 V and 1.319 V, as displayed in Fig. 8. A voltage of 1.287 V at 0.662 A cm^{-2} corresponds to the thermoneutral voltage, which is slightly above the theoretic value obtained from the standard Gibbs free energy change of reaction in order to balance the thermal losses through the unit insulation.

Since the electrolyser unit is composed of 10,000 cells, the corresponding unit power ranges from 633 kW to 1101 kW. As shown in Fig. 9, the electrolyser unit efficiency decreases from 118%

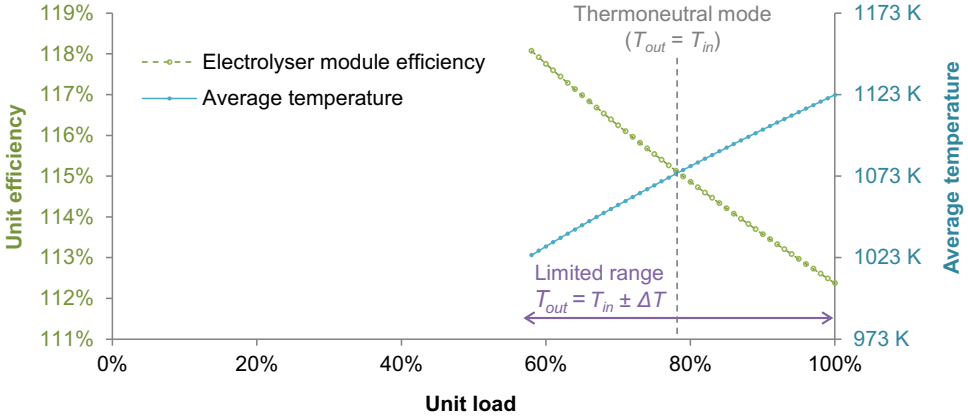

Fig. 9. Electrolyser unit efficiency and average temperature as a function of the unit load in steady state.

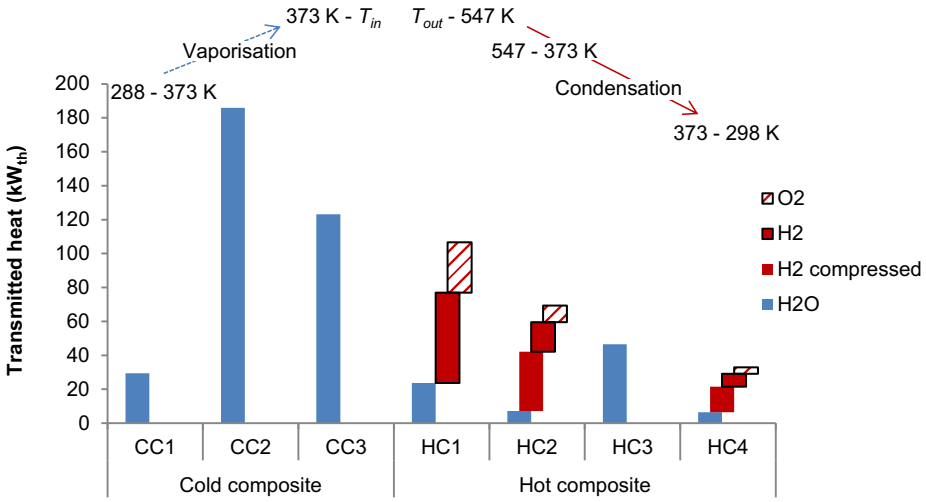

Fig. 10. Inlet (cold composite) and outlet (hot composite) gases thermal requirements at the thermoneutral power in steady state.

vs. HHV at the minimum load (633 kW, endothermic mode) to 112.3% vs. HHV at the maximum load (1101 kW, exothermic mode). In the thermoneutral mode (852 kW), a 115.2% efficiency vs. HHV is achieved, which is coherent with the theoretical value obtained from the enthalpy change of reaction. The produced hydrogen flows out of the electrolyser module at a rate of 19 kg h^{-1} and a temperature of 973 K at 633 kW, and increases to a rate of 31.4 kg h^{-1} and a temperature of 1173 K at 1101 kW.

3.2. Pinch analysis

In the thermoneutral mode, 297 kg h^{-1} of water at 288 K have to be vaporised and overheated to 1073 K before entering the electrolyser module, whereas 25 kg h^{-1} of produced hydrogen, 198 kg h^{-1} of produced oxygen and 74 kg h^{-1} of unreacted steam require cooling from 1073 K to 298 K. Once cooled down, the produced hydrogen is compressed from 0.1 to 3 MPa in two stages, implying that 25 kg h^{-1} of hydrogen requires two additional cooling steps from 547 K to 298 K.

Fig. 10 displays the thermal energy required for each cooling and heating steps at the thermoneutral power. The inlet water is heated from 288 K (T_{source}) to 373 K (CC1), before being vaporised (CC2) and overheated from 373 K to 1073 K (T_{in}) (CC3). It is important to notice that the vaporisation and overheating needs represent, respectively, 55% and 36% of the total thermal needs for the inlet stream (338 kW$_{th}$).

The outlet streams are cooled down from 1073 K (T_{out}) to 547 K ($T_{c,2}$) (HC1). Below 547 K ($T_{c,2}$), additional compressed hydrogen has to be cooled down. The outlet gases and the additional compressed hydrogen are cooled down from 547 K ($T_{c,2}$) to 373 K (HC2), steam is condensed at 373 K (HC3), and gases are further cooled down from 373 K to 298 K (HC4). Steam condensation represents 18% of the total cooling needs (255 kW$_{th}$) since 25% of the inlet steam did not react. Hydrogen represents 50% of the cooling needs, 20% being related to the compression.

Due to the flow rates increasing with the current, both the cold and the hot needs increase from the endothermic to the exothermic mode, as shown in Fig. 11. The total BoP thermal requirements increase from 141 kW$_e$ (125 kW$_{th}$ heating and 50 kW$_{th}$ cooling) at the minimum power to 187 kW$_e$ (167 kW$_{th}$ heating and 83 kW$_{th}$ cooling) at the maximum power. Independently from the operating mode, both inlet and outlet gases flow out of the heat recovery system with a temperature of 373 K, the inlet gases being further heated to 1073 K electrically and the outlet gases being cooled down to 298 K by pumped cooling water. The percentage of inlet water that is vaporised by the heat recovery is ranged from 80% to 95%, whereas only 30% of the outlet steam is condensed by the inlet water.

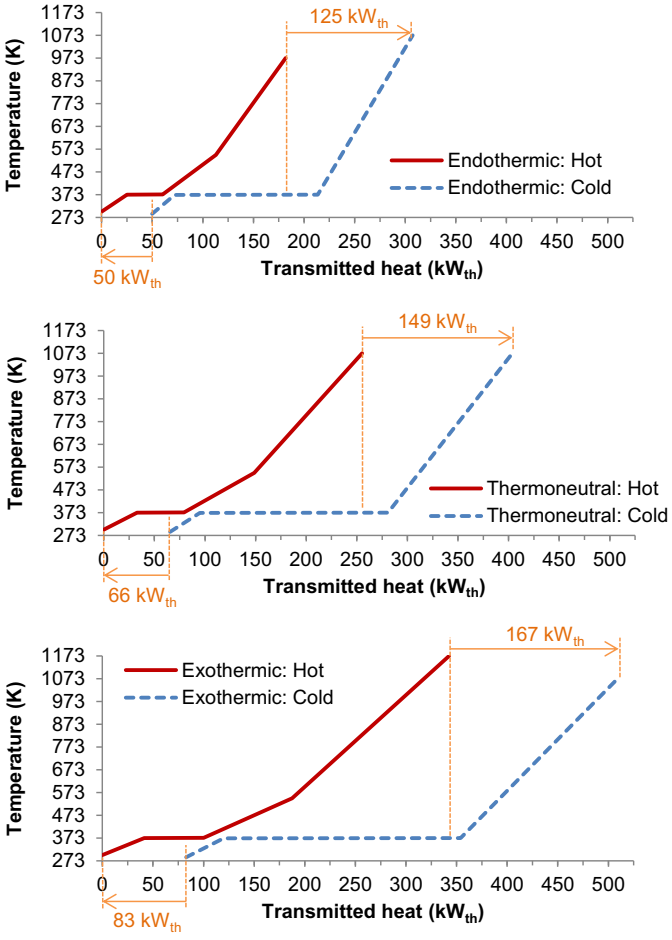

Fig. 11. Combined composite curves of the pinch analysis at the minimum (top), thermoneutral (middle) and maximum (bottom) power in steady state.

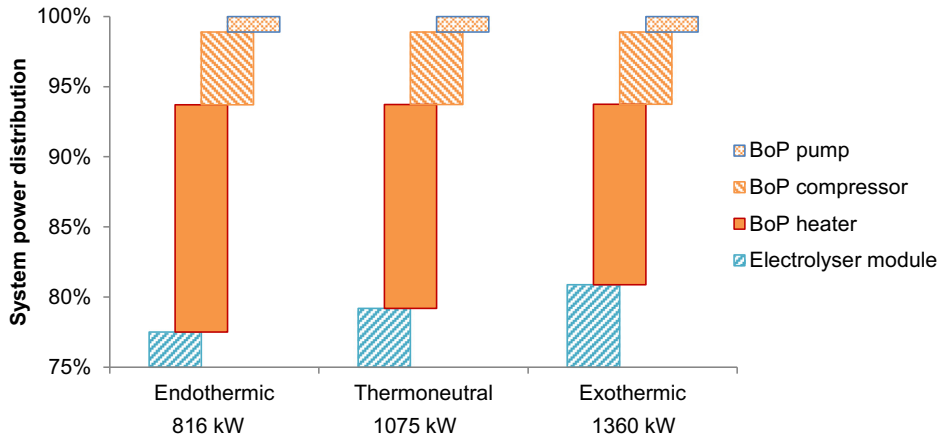

Fig. 12. System power requirements distribution among the electrolyser module, the BoP heater, the BoP compressor and the BoP pump at the minimum, thermoneutral and maximum load in steady state.

3.3. System power and efficiency

Apart from the electrolyser (78–81% of the system power), the BoP electrical heater (13–16% of the system power) is the most power consuming component since water is 5–20% vaporised and entirely overheated from 373 K to 1073 K electrically. This is coherent with results of Rivera-Tinoco et al. [18] who obtained contributions of 85% for the electrolyser and 15% for heating. This result confirms that an external heat source would significantly increase the system efficiency, as it is considered in most studies [16–18]. On the contrary, the compressor power represents only 5% of the total power, as shown in Fig. 12.

It is important to notice that the excess heat dissipated in the exothermic mode is partly compensated by a decrease in the BoP heater consumption. In the endothermic mode, the reaction thermal needs are partly compensated by the BoP heater through an increase in the consumption. Due to this, although the cell efficiency highly depends on the operating mode and equals $115 \pm 3\%$ vs. HHV, the system efficiency is only slightly impacted by the unit load and equals $91.2 \pm 0.4\%$ vs. HHV, as shown in Fig. 13. Therefore, although no external heat source is provided and hydrogen compression is performed in the BoP, the SOEC system has a higher efficiency than low temperature electrolysis technologies.

Works of O'Brien et al. [16] considered an SOEC system operating at 3.5 MPa and directly fed with steam at 920 K. Works of Quandt et al. [17] considered an SOEC system operating at 0.4 ± 0.1 MPa and directly fed with steam at 473 K. Data collected in these studies have been converted to facilitate comparison in Table 2. In both studies, a nuclear reactor generated heat (600 MW_{th} and 451 MW_{th}, respectively), which was mostly (540 MW_{th} and 421 MW_{th}, respectively) converted into electricity (284 MW_e and 160 MW_e, respectively) to power the electrolyser. The produced hydrogen rate was 8.3 ton h^{-1} and 4.5 ton h^{-1}, respectively. The electrical power is assumed to cover the consumption of the BoP components, such as the pumps, although no detailed information was provided. The remaining heat (60 MW_{th} and 30 MW_{th}, respectively) was used to preheat the reacting steam to 920 K [16] and 473 K [17], respectively. For an accurate comparison with the results of the present study, the heat used to preheat the reacting steam is assumed to be provided by an electrical heater with an efficiency of 95% rather than by a nuclear reactor, which corresponds to a heater power of 63 MW_e and 32 MW_e, respectively. Finally, the sum of the specific electrical consumption and the specific heater consumption can be compared with the HHV (39.41 kWh kg^{-1}) to calculate the system efficiency.

Hydrogen compression from the atmospheric pressure to 3 MPa in the present study might explain the lower system efficiency (91.0% vs. HHV) and the higher specific electrical consumption (38 kWh_e kg^{-1}), whereas the lower specific heater consumption (5.6 kWh_e kg^{-1}) might be due to two factors. First, the recovery of the compression heat enables to lower the BoP requirements. Moreover, preheating the inlet steam to 920 K [16] or 473 K [17] might not be optimised.

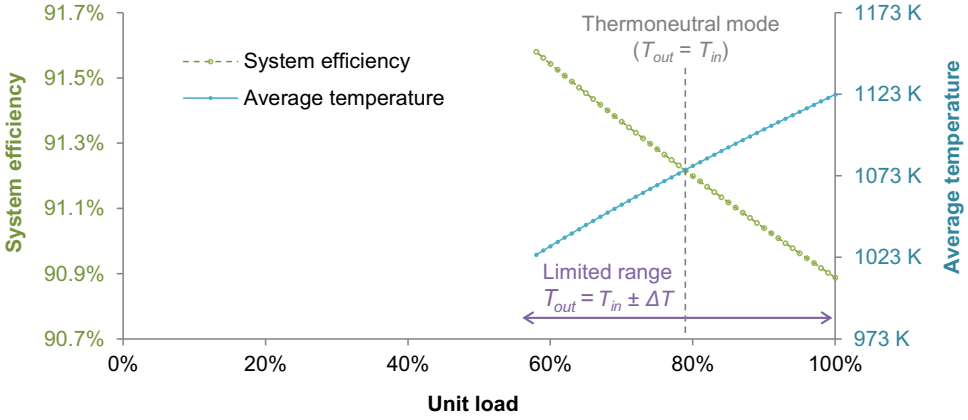

Fig. 13. System efficiency and average temperature as a function of the unit load in steady state, limited to 57–100% without control strategy.

Table 2
Comparison of the results with results presented in Refs. [16,17].

	O'Brien et al. [16]	Quandt et al. [17]	Present study
Cell voltage (V)	1.37[b]	1.32[a]	1.32
Operating pressure (MPa)	3.5[a]	0.3–0.5[a]	0.1
Total thermal power (kW_{th})	600,000[a]	451,053[b]	
Total electrical power (kW_e)			1360
Electrical requirements	90%[a]	93%[b]	
Electrical power (kW_{th})	540,000[b]	421,053[b]	
Power generation efficiency	52.6%[a]	38.0%[a]	
Electrical power (kW_e)	284,040[b]	160,000[b]	1184
Electrical energy ($kWh_e\,m^{-3}$)		3.2[a]	
Heating requirements	10%[a]	7%[b]	
Heating power (kW_{th})	60,000[b]	30,000[b]	167
Heating energy ($kWh_{th}\,m^{-3}$)		0.6[a]	
Heater efficiency	95%[c]	95%[c]	95%
Heater power (kW_e)	63,158[b]	31,579[b]	176
Heater energy ($kWh_e\,m^{-3}$)		0.63[b]	
Hydrogen production rate ($kg\,h^{-1}$)	8280[a]	4500[a]	31.40
Specific electrical consumption ($kWh_e\,kg^{-1}$)	34.30[b]	35.56[b]	37.71
Specific heater consumption ($kWh_e\,kg^{-1}$)	7.63[b]	7.02[b]	5.61
System efficiency (vs. HHV)	94.0%[b]	92.6%[b]	91.0%

[a] Given in the reference paper.
[b] Calculated.
[c] Assumed for accurate results comparison.

3.4. Options to enlarge the operating power range

The system power ranges from 816 kW (corresponding to the minimum unit power of 633 kW) to 1360 kW (corresponding to the maximum unit power of 1101 kW), which corresponds to a system power load in the range 60–100%, whereas the unit power load is in the range 57–100%. Below 60% load (minimum system power), the electrolyser unit temperature would decrease below 1023 K, which would threaten the cells mechanical integrity.

In Solid Oxide Fuel Cell (SOFC) systems, which operate around 1073 K with similar cells, thermal issues are managed both directly, via electrical heaters, and indirectly, via air sweep. During the cold start-up phase, the SOFC system is heated from the ambient temperature to the operating temperature by electrical heaters which are placed all around the stacks and respect a prescribed heat-up rate in order to not damage the stack components through thermal gradients. Once the SOFC system has reached the operating temperature, it is operated and heat dissipated by the exothermic reaction is evacuated via a high air sweep at the oxygen electrode.

In an SOEC system, the main challenge is thermal management at partial load due to the endothermic mode. Both strategies of using electrical heaters and air sweep at the oxygen electrode can be considered. A further strategy could be the use of several independently operated electrolyser units. In the presented case of one electrolyser unit, the system power load is limited to 60–100%, whereas four electrolyser units could enlarge the system load range to 15–100%.

Regulating the cell temperature with air sweep has been studied by Udagawa et al. [19] at the cell level. This control strategy as well as both further strategies presented above should be studied at the system level in order to identify their impact on the system design and efficiency.

4. Conclusions

The dynamic model of a high temperature electrolyser system is presented and run in steady state in order to observe the behaviour of an SOEC system operated at different loads. In the Balance of Plant, hydrogen is compressed from the atmospheric pressure to 3 MPa, and high temperature steam is entirely generated through heat recovery combined with electrical heating. The results show that the system efficiency reaches 91% vs. HHV, which is higher than for pressurised low temperature electrolysers.

However, given the ceramic materials thermal constraints, the maximum tolerated temperature gradient across the cells is $\pm$ 100 K, which restricts the average operating temperature to the range 1073 $\pm$ 50 K. Because the temperature is load dependent, this leads to a limited system power load of 60–100%. It is concluded that control strategies, such as electrical heating, electrode air sweep and modular operation, should be implemented to enlarge the load range and make the high temperature electrolyser system suitable for variable operation.

Acknowledgements

The authors thank the partners of the European funded ADEL project (grant no. 256755) for the fruitful collaboration.

References

[1] The Outlook for Energy: A View to 2040, Exxon Mobil, Irving, 2012.
[2] J. Wilkes, J. Moccia, M. Dragan, Wind in Power: 2011 European Statistics, EWEA, Brussels, 2012.
[3] R. Goldstein, W. MacDougall, Hydrogen and Power-to-gas Technology, Germany Trade & Invest, Berlin, 2012.
[4] H. Derbal-Mokrane, A. Benzaoui, A. M'Raoui, M. Belhamel, Int. J. Hydrogen Energy 36 (2011) 4198–4207.
[5] O. Bucheli, F. Lefebvre-Joud, F. Petipas, M. Roeb, M. Romero, in: Proceedings of the 10th European SOFC Forum, Lucerne, 2012.
[6] A. Houaijia, N. Monnerie, M. Roeb, C. Sattler, J. Sanz-Bermejo, M. Romero, I. Canadas, A. Drisaldi Castro, C. Lucero, R. Palomino, F. Petipas, A. Brisse, in: Proceedings of the Solar PACES 2012, Marrakech, 2012.
[7] F. Petipas, Q. Fu, A. Brisse, C. Bouallou, Int. J. Hydrogen Energy 38 (2013) 2957–2964.
[8] J. Udagawa, P. Aguiar, N.P. Brandon, J. Power Sources 166 (2007) 127–136.
[9] M. Ni, M.K.H. Leung, D.Y.C. Leung, Int. J. Hydrogen Energy 32 (2007) 2305–2313.
[10] R. Rivera.Tinoco, Techno-economic Study of Hydrogen Production by High Temperature Electrolysis Coupled with Different Thermal Energy Sources, Ph.D. thesis, France, 2009.
[11] J.E. O'Brien, C.M. Stoots, G.L. Hawkes, in: Proceedings of the 2005 ASME International Mechanical Engineering Congress and Exposition, Orlando, 2005.
[12] Q. Fu, C. Mabilat, M. Zahid, A. Brisse, L. Gautier, Energy Environ. Sci. 3 (2010) 1382–1397.
[13] J.E. O'Brien, in: 19th World Hydrogen Energy Conference, June, Toronto, 2012. http://www.whec2012.com/wp-content/uploads/2012/06/WHEC-HTE-OBrien.pdf (accessed 27.02.13).
[14] H. Apfel, M. Rzepka, H. Tu, U. Stimming, J. Power Sources 154 (2006) 370–378.
[15] M. Sorrentino, C. Pianese, Y.G. Guezennec, J. Power Sources 180 (2008) 380–392.
[16] J.E. O'Brien, M.G. McKellar, E.A. Harvego, C.M. Stoots, Int. J. Hydrogen Energy 35 (2010) 4808–4819.
[17] K.H. Quandt, R. Streicher, Int. J. Hydrogen Energy 11 (1986) 309–315.
[18] R. Rivera-Tinoco, C. Mansilla, C. Bouallou, Energ. Convers. Manage. 51 (2010) 2623–2634.
[19] J. Udagawa, P. Aguiar, N.P. Brandon, J. Power Sources 180 (2008) 354–364.
[20] A. Nakajo, Z. Wuillemin, J. Van Herle, D. Favrat, J. Power Sources 193 (2009) 203–215.
[21] A. Brisse, J. Schefold, M. Zahid, J.U. Nielsen, P. Noyé, in: Proceedings of the Nineth Lucerne Fuel Cell Forum, Lucerne, 2010.
[22] The National Institute of Standards and Technology Chemistry WebBook. http://webbook.nist.gov/chemistry/fluid/ (accessed 27.02.13).
[23] A. Stubinitzky, Advanced H_2 fuelling & compression technologies – Experienced gained and technology improvements. http://www.whec2012.com/wp-content/uploads/2012/07/NEW-ASR14.1.pdf, 2013 (accessed 27.02.13).
[24] S. Yun, S. Ted Oyama, J. Membrane Sci. 375 (2011) 28–45.
[25] Online pinch analysis tool. http://www.uic-che.org/pinch/about_program.php (accessed 27.02.13).
[26] A. Franco, N. Giannini, Energy 31 (2006) 3342–3361.